

Article

Design of Active Disturbance Rejection Controller for Trajectory-Following of Autonomous Ground Electric Vehicles

Xianjian Jin ^{1,2,*}, Huaizhen Lv ¹, Zhihui He ^{3,*}, Zhiwei Li ¹, Zhaoran Wang ¹ and Nonsly Valerienne Opinat Ikiela ¹

¹ School of Mechatronic Engineering and Automation, Shanghai Key Laboratory of Intelligent Manufacturing and Robotics, Shanghai University, Shanghai 200072, China

² State Key Laboratory of Automotive Simulation and Control, Jilin University, Changchun 130025, China

³ School of Marine Engineering Equipment, Zhejiang Ocean University, Zhoushan 316022, China

* Correspondence: xianjianjin@shu.edu.cn (X.J.); 2022156@zjyou.edu.cn (Z.H.)

Abstract: In this paper, the concept of symmetry is utilized in the promising trajectory-following control design of autonomous ground electric vehicles—that is, the construction and the solution of active disturbance rejection controllers are symmetrical. This paper presents an active disturbance rejection controller (ADRC) for improving the trajectory-following performance of autonomous ground electric vehicles (AGEV) with an advanced active front steering system. Since AGEV trajectory dynamics are inherently affected by complex traffic conditions, various driving maneuvers, and other road environment, the main control objective is to deal with the AGEV trajectory control challenges of system uncertainties, system nonlinearities, and external disturbance. First, the vehicle dynamics trajectory-following model and its state space representation system are established. Then, the augmented control-oriented vehicle-trajectory-following system with dynamic error is developed. The resulting active disturbance rejection controller of the vehicle-trajectory-following system is finally designed using the trajectory performance index and active disturbance compensation, and the stability of the active disturbance rejection controller is also analyzed and derived via Lyapunov stability theory. The effectiveness of the proposed controller is validated through double lane change and serpentine maneuvers under the co-simulation platform of MATLAB/Simulink-Carsim[®]. Simulation results show that the designed controller provides enhanced vehicle-trajectory-following performance compared to the linear quadratic regulator controller (LQR) and model predictive controller (MPC). It will provide a certain guidance for the controller engineering design of the AGEV trajectory-following system.

Keywords: autonomous ground electric vehicle; active disturbance rejection controller; extended state observer; trajectory-following control



Citation: Jin, X.; Lv, H.; He, Z.; Li, Z.; Wang, Z.; Ikiela, N.V.O. Design of Active Disturbance Rejection Controller for Trajectory-Following of Autonomous Ground Electric Vehicles. *Symmetry* **2023**, *15*, 1786. <https://doi.org/10.3390/sym15091786>

Academic Editor: Christos Volos

Received: 23 August 2023

Revised: 13 September 2023

Accepted: 16 September 2023

Published: 18 September 2023



Copyright: © 2023 by the authors. Licensee MDPI, Basel, Switzerland. This article is an open access article distributed under the terms and conditions of the Creative Commons Attribution (CC BY) license (<https://creativecommons.org/licenses/by/4.0/>).

1. Introduction

In recent years, the rapid development of autonomous ground electric vehicles (AGEV) has captured the attention of numerous experts [1,2]. AGEV possess advantages in terms of environmental friendliness, safety, and convenience, which can contribute to reducing environmental pollution, alleviating traffic congestion, enhancing road safety, and significantly improving the convenience of people's transportation [1–4]. Active front steering system (AFS), as a crucial control component in trajectory-following control, is one of the key focuses in the application of active chassis control technology for the steering system of AGEV. Indeed, effective AFS control can enhance passenger comfort, vehicle stability, and safety during travel. With considerations of driver safety, maneuverability, and trajectory tracking performance, integrating an AFS system in AGEV will offer substantial benefits [5]. AFS's intrinsic characteristics, such as its quick reactivity and exact execution, can also be dedicated to AGEV's active safety and brilliant trajectory-tracking performance [4–8].

The trajectory-following control problem for AGEV still faces some challenges such as system nonlinearity, and internal and external disturbances, especially in curved road

conditions. These issues in AGEV trajectory-following control lead to decreased stability, slower response speed, reduced control precision, and steady-state error in the control system. AGEV must accurately follow the desired path to avoid significant deviations that can cause unexpected accidents, it is essential to maintain vehicle stability and safety to prevent rollovers, skidding, and collisions. To address the challenges faced by the AGEV trajectory-following control system, different control strategies—such as model predictive control [9–11], robust control [12,13], reliable fuzzy control [14], sliding mode control [15], and other nonlinear methods [16,17]—have been developed. This model predictive controller (MPC) approach is proposed to address the mutual interference in [9]. It utilized tire force redistribution for both braking and steering control to accurately follow the desired trajectory. In [11], the constrained MPC of dynamic path tracking is presented in terms of the road geometry parameters and the slippage-friction conditions at the wheel–ground contacts; simulations and experiments on a real off-road vehicle verified that the designed controller can reach the desired path for different kinds of trajectories and velocity levels. In [12], a robust H-infinity network observer-based path tracking control of the augmented AGEV system is designed to reduce the effect of measurement noise, sensor attack signals, and external disturbance, which can attenuate unknown disturbance for the energy of path tracking error by using state and attack estimation. The study [14] considered the road curvature disturbance of path following control for AGV; the road–vehicle dynamics model is constructed using Takagi–Sugeno (T-S) fuzzy form, then the fuzzy control is used as a new solution to avoid road curvature disturbance. Both theoretical simulations and hardware experiments demonstrated the solution under real driving situations. In [15], a sliding mode control (SMC)-based path-tracking algorithm with model-free adaptive feedback action is presented for autonomous vehicles. Adaptive feedback control (AFC) and SMC are integrated to adjust the bounded uncertainty by taking into account the sliding surface and unknown uncertainty. Based on an uncertain dynamic model expressed as nonlinear ordinary differential equations, the work [17] proposed the nonlinear MPC (NMPC) strategy considering the state and the control constraints that significantly affect the system’s safety and stability. Then, the NMPC problem is solved using validated simulation and interval analysis methods, and its capabilities are illustrated through several simulations.

Despite the aforementioned developments in trajectory-following control, how to deal with AGEV system nonlinearity and internal and external disturbances remain as difficulties. Recently, ADRC technology has been shown to possess the ability to deal with these challenges, and the ADRC retains the advantages of simple computation, structural simplicity strong versatility, and strong robustness against disturbance compensation, which can improve system stability, reliability, and response speed [18–24]. Recently, several efforts have been brought forward in this respect. An active disturbance rejection controller is introduced in active suspension system control of half-tracked vehicle, total disturbances can be eliminated by switch extended state observer [21]. In [23], a dual-loop control strategy based on active disturbance rejection control is designed to attenuate external and internal disturbances of single-stage three-phase isolated matrix rectifiers (TIMRs). The work [24] studied cascade active disturbance rejection control for trajectory-tracking control of a quadrotor unmanned aerial vehicle in terms of external disturbances and model uncertainties; the controller was designed by decomposing the attitude dynamic system into two serially connected subsystems.

In this paper, a new trajectory-following active disturbance rejection controller of AGEV is designed to deal with problems such as system nonlinearity, uncertainties, and disturbances. Firstly, the AGEV dynamic model and its state space representation are established. Subsequently, to achieve desirable control performance, an active disturbance rejection controller to estimate and compensate for AGEV unknown disturbances is designed. Finally, the combined simulation platform of MATLAB/Simulink/Carsim is used to validate the effectiveness of the ADRC controller under double lane change and serpentine maneuvers.

2. Vehicle-Trajectory-Following Model

To facilitate computation and analysis, this paper constructs a bicycle model to investigate the dynamic characteristics of the AGEV. Here assumptions are made using the bicycle model: the suspension is a robust construction, and the slip angle is usually small under normal driving conditions. The bicycle model is used as a tool in the examination of actual vehicle movements [5,7,25,26]. The essential parameters and symbols show in Appendix A.

$$\begin{cases} m_{AGEV}(\dot{\mu}_x - v_y\dot{\varphi}) = F_{f-y} \sin \delta_f + F_{f-x} \cos \delta_f + F_{r-x} \\ m_{AGEV}(\dot{y} + \mu_x\dot{\varphi}) = F_{f-y} \cos \delta_f + F_{f-x} \sin \delta_f + F_{r-y} \\ I_z\ddot{\varphi} = l_f(F_{f-y} \cos \delta_f + F_{f-x} \sin \delta_f) - l_r F_{r-y} \end{cases} \quad (1)$$

According to Newton's law, the lateral dynamic equation along the Y-axis and the yaw kinematic equation of the vehicle around the Z-axis can be expressed as follows:

$$m_{AGEV}\dot{v} \sin \beta + m_{AGEV}v(\dot{\beta} + \dot{\varphi}) \cos \beta = F_y \quad (2)$$

$$I_z\ddot{\varphi} = M_z \quad (3)$$

This model includes variables such as lateral force F_y , yaw angle φ , yaw torque M_z , moment of inertia I_z , mass m , and side-slip angle β .

The lateral acceleration and the angular acceleration can be expressed as:

$$a_y = \dot{v} \sin \beta + v(\dot{\beta} + \dot{\varphi}) \cos \beta = \frac{d}{dt}(v \sin \beta) + v \cos \beta \dot{\varphi} = \mu_x - v_y\dot{\omega}_r \quad (4)$$

$$\ddot{\varphi} = \frac{d}{dt}\dot{\varphi} = \dot{\omega}_r \quad (5)$$

The variables of this model, such as lateral velocity ϑ_y , longitudinal velocity μ_x , and angular velocity $\dot{\omega}_r$. The side-slip angle β can be expressed using the lateral and longitudinal velocities:

$$\tan \beta = \frac{v_y}{\mu_x} \quad (6)$$

The external force exerted on the vehicle along the Y-axis and the moment applied around the Z-axis can be respectively represented as follows:

$$F_y = F_{f-y} \cos \delta_f + F_{f-x} \sin \delta_f + F_{r-y} \quad (7)$$

$$M_z = l_f(F_{f-y} \cos \delta_f + F_{f-x} \sin \delta_f) - l_r F_{r-y} \quad (8)$$

where F_{iy} , F_{ix} represent lateral tire forces and longitudinal tire forces, respectively.

In this paper, only the front wheels serve as steering wheels. The slip angles of the front and rear axles can be expressed as:

$$\begin{cases} \alpha_{f\tau} = \delta_f - \arctan(\tan \beta + \frac{l_f\omega_r}{\mu_x}) \\ \alpha_{r\tau} = -\arctan(\tan \beta - \frac{l_r\omega_r}{\mu_x}) \end{cases} \quad (9)$$

By combining the aforementioned equations, the bicycle model of AGEV can be represented as follows:

$$\begin{cases} \dot{v}_y = -\mu_x\dot{\omega}_r + \frac{F_{f-y} \cos \delta_f + F_{r-y}}{m_{AGEV}} \\ \dot{\omega} = \frac{l_f F_{f-y} \cos \delta_f - l_r F_{r-y}}{I_z} \end{cases} \quad (10)$$

From the equation, the nonlinearity of the simplified lateral dynamics model arises due to the presence of tire lateral forces and trigonometric functions. The complexity introduced by the nonlinear model presents challenges for the development of the control system. It leads to prolonged equation-solving times, which in turn hampers the real-time

responsiveness of the control system. Assuming that during AGEV movement, both the wheel angle and side-slip angle remain small, the trigonometric functions can be simplified as $\cos x \approx 1$, $\sin x \approx x$. Then, the tire slip angles of the front and rear axles can be simplified as:

$$\begin{cases} \alpha_{f\tau} = \delta_f - \beta + \frac{l_f w_r}{\mu_x} \\ \alpha_{r\tau} = -\beta + \frac{l_f w_r}{\mu_x} \end{cases} \quad (11)$$

The lateral force of the tire is linearly proportional to the tire slip angle under the premise that is modeled during driving circumstances.

Furthermore, we assume AGEV only travels in the horizontal plane, ignoring the influence of other factors. Consequently, based on Equation (11), it can be rewritten:

$$\begin{bmatrix} \dot{v}_y \\ \dot{w}_r \end{bmatrix} = A_L \begin{bmatrix} v_y \\ w_r \end{bmatrix} + B_L \delta_f + \tau \quad (12)$$

$$A_L = \begin{bmatrix} -\frac{\bar{N}_{C_f} + N_{C_r}}{m_{AGEV}\mu} & -\mu + \frac{\bar{N}_{C_r} l_r - \bar{N}_{C_f} l_f}{m_{AGEV}\mu} \\ \frac{\bar{N}_{C_r} l_r - \bar{N}_{C_f} l_f}{I_z \mu} & -\frac{\bar{N}_{C_r} l_r^2 + \bar{N}_{C_f} l_f^2}{I_z \mu} \end{bmatrix}, B_L = \begin{bmatrix} \bar{N}_{C_f} \\ \frac{m_{AGEV}}{\bar{N}_{C_f} l_f} \end{bmatrix}, \tau = \begin{bmatrix} \tau_2 \\ \tau_4 \end{bmatrix}$$

where τ_2 and τ_4 represent the model state error.

Figure 1 summarizes the AGEV’s trajectory-following progress. The desired yaw angle is denoted by φ_r . The derivatives of y_e and φ_e can be expressed as:

$$\begin{cases} \dot{y}_e = \mu_x - v_y \varphi_e \\ \dot{\varphi}_e = \dot{\varphi} - \dot{\varphi}_r \end{cases} \quad (13)$$

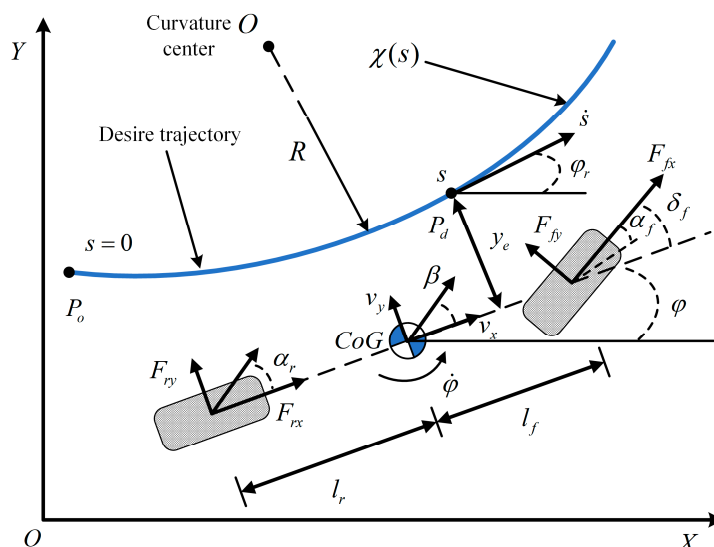


Figure 1. The AGEV trajectory-following procedure.

The derivatives information of s can be expressed as:

$$\begin{cases} \dot{s} = \mu_x + v_y \varphi_e \\ \ddot{s} = \dot{\mu}_x + \dot{v}_y \varphi_e + v_y \dot{\varphi}_e \end{cases} \quad (14)$$

cast into a state space representation:

$$\dot{x} = Ax + Bu + B_\tau \tau \quad (15)$$

where

$$A = \begin{bmatrix} 0 & 1 & 0 & 0 \\ 0 & -\frac{\bar{N}_{C_f} + \bar{N}_{C_r}}{m_{AGEV}\mu} & \frac{\bar{N}_{C_f} + \bar{N}_{C_r}}{m_{AGEV}} & -\frac{l_f \bar{N}_{C_f} - l_r \bar{N}_{C_r}}{m_{AGEV}\mu} \\ 0 & 0 & 0 & 1 \\ 0 & -\frac{l_f \bar{N}_{C_f} + l_r \bar{N}_{C_r}}{I_z \mu} & \frac{l_f \bar{N}_{C_f} + l_r \bar{N}_{C_r}}{I_z} & -\frac{l_f^2 \bar{N}_{C_f} + l_r^2 \bar{N}_{C_r}}{I_z \mu} \end{bmatrix},$$

$$x = \begin{bmatrix} y_e \\ \dot{y}_e \\ \varphi_e \\ \dot{\varphi}_e \end{bmatrix}, B_\tau = \begin{bmatrix} 0 \\ 1 \\ 0 \\ 1 \end{bmatrix}^T, B = \begin{bmatrix} 0 \\ \frac{\bar{N}_f}{m_{AGEV}} \\ 0 \\ \frac{l_f \bar{N}_f}{I_z} \end{bmatrix},$$

3. Active Disturbance Rejection Controller Design

3.1. ADRC Structure

The ADRC controller is a novel and practical digital control technique that does not rely on an accurate model of the system. It consists of three components: TD, NLSEF, and ESO.

The TD module is designed to manage the transitional process. When implementing the ADRC controller, it is essential to pre-arrange an appropriate transitional process based on the system's tolerance capacity. This effectively lessens the harm that the noise amplification effect causes. A second order can be designed as follows:

$$\begin{cases} s_{TD,1}(k+1) = s_{TD,1}(k) + h s_{TD,2}(k) \\ s_{TD,2}(k+1) = s_{TD,2}(k) h * fh \\ fh = fhan(s_{TD,1}(k) - v(k), s_{TD,2}(k), r, h) \end{cases} \quad (16)$$

where s_1 is the trajectory and s_2 is its derivative.

The ESO is utilized for observing the system's output, estimating disturbances, and compensating for these disturbances in the control signal. This type of disturbance compensation is achieved through the specific implementation of feedback linearization for uncertain systems. The structure of the third-order ESO is given as:

$$\begin{cases} \tau = z_{E,k1} - y \\ \dot{z}_{E,k1} = z_{E,k2} - \alpha_1 \tau \\ \dot{z}_{E,k2} = z_{E,k3} - \alpha_2 fl(e, 0.5, h) + bu \\ \dot{z}_{E,k3} = \alpha_3 fl(e, 0.25, h) \end{cases} \quad (17)$$

where α_k ($k = 1, 2, 3$) is the gains of the ESO. z_{k3} represents the total disturbance estimation of the system. With this estimation of the total disturbance, the entire control problem, as discussed in the preceding process, simplifies into a straightforward error feedback problem.

Through NLFSE, we can obtain the initial control input.

$$\begin{cases} e_1 = s_{TD,1} - z_{E,k1} & e_2 = s_{TD,2} - z_{E,k2} \\ u_0 = fhan(e_1, ce_2, r, h_1) \end{cases} \quad (18)$$

To obtain the final control input for the system, we combine the initial control input and the disturbance component estimated by ESO.

$$u = \frac{(u_0 - z_{E,k3})}{b_0} \quad (19)$$

where b_0 is the compensation factor.

3.2. ADRC Design

We assume that the vehicle's longitudinal velocity will remain constant in the design of the lateral controller to allow it to track the desired path that the planning layer provides effectively. Variations in velocity are treated as external disturbances to the lateral controller. The ESO can compensate for the component of the overall disturbance to the controller that causes instability in lateral control due to changes in velocity. Consequently, by controlling the lateral displacement error y_e and the yaw angle error φ_e , it is possible to approach zero tracking error.

Note that MPC can offer advantages in handling multi-input, multi-output models. By utilizing state-space models and MPC, the design of the error feedback control law for ADRC can be achieved.

Choosing x as the state variable and u as the control input. For the controller design, selecting a sampling time of T_s seconds, the continuous-time state-space equations of the system are discretized using the Euler method as follows:

$$\dot{\tilde{x}} = \frac{\tilde{x}_{k+1} - \tilde{x}_k}{T_s} = Ax + Bu \quad (20)$$

$$\begin{cases} \tilde{x}_{k+1} = (T_s A + E)\tilde{x}_k = A_{T_s}\tilde{x}_k + B_{T_s}u_k \\ \tilde{y}_{k+1} = C_{T_s}\tilde{x}_{k+1} \end{cases} \quad (21)$$

According to the principles and rules, the future vehicle states can be obtained through (21). The prediction horizon is \tilde{N}_p and the control horizon is \tilde{N}_c , while simultaneously satisfying $\tilde{N}_p \geq \tilde{N}_c$.

We can obtain:

$$\begin{cases} \tilde{x}_{p,k+1} = A_{T_s}\tilde{x}_{p,k} + B_{T_s}u_{p,k} \\ \tilde{x}_{p,k+2} = A_{T_s}^2\tilde{x}_{p,k} + A_{T_s}B_{T_s}u_{p,k} + B_{T_s}u_{p,k+1} \\ \tilde{x}_{p,k+3} = A_{T_s}^3\tilde{x}_{p,k} + A_{T_s}^2B_{T_s}u_{p,k} + A_{T_s}B_{T_s}u_{p,k+1} + B_{T_s}u_{p,k+2} \\ \dots \\ \tilde{x}_{p,k+\tilde{N}_p} = A_{T_s}^{\tilde{N}_p}\tilde{x}_{p,k} + A_{T_s}^{\tilde{N}_p-1}B_{T_s}u_{p,k} + \dots + A_{T_s}^{\tilde{N}_p-\tilde{N}_c}B_{T_s}u_{p,k+\tilde{N}_c-1} \end{cases} \quad (22)$$

Predicted output:

$$\begin{cases} \tilde{y}_{p,k+1|k} = C_{T_s}A_{T_s}\tilde{x}_{p,k} + C_{T_s}B_{T_s}u_{p,k} \\ \tilde{y}_{p,k+2|k} = C_{T_s}A_{T_s}^2\tilde{x}_{p,k} + C_{T_s}A_{T_s}B_{T_s}u_{p,k} + C_{T_s}B_{T_s}u_{p,k+1} \\ \tilde{y}_{p,k+3|k} = C_{T_s}A_{T_s}^3\tilde{x}_{p,k} + C_{T_s}A_{T_s}^2B_{T_s}u_{p,k} + C_{T_s}A_{T_s}B_{T_s}u_{p,k+1} + C_{T_s}B_{T_s}u_{p,k+2} \\ \dots \\ \tilde{y}_{p,k+\tilde{N}_p|k} = C_{T_s}A_{T_s}^{\tilde{N}_p}\tilde{x}_{p,k} + C_{T_s}A_{T_s}^{\tilde{N}_p-1}B_{T_s}u_{p,k} + \dots + C_{T_s}A_{T_s}^{\tilde{N}_p-\tilde{N}_c}B_{T_s}u_{p,k+\tilde{N}_c-1} \end{cases} \quad (23)$$

Constructing the objective function:

$$J(\tilde{X}_{p,k}, u_{p,k-1}) = \sum_{i=1}^{\tilde{N}_p} \|\tilde{y}_{p,k+i|k} - s_{ref}(k+i, k)\|^2 + \sum_{i=0}^{\tilde{N}_c-1} \|u_{p,k+i}\|^2 \quad (24)$$

Due to the mechanical design and limitations of the front wheel steering actuator, there are constraints on the control output, specifically the rate of change of the front wheel steering angle $\Delta\delta_f$:

$$\Delta\delta_{p,f}^{\min} \leq \Delta\delta_{p,f}(k+i) \leq \Delta\delta_{p,f}^{\max}, i = 1, 2, \dots, N_c \quad (25)$$

Due to the saturation characteristics of tires as the primary cause of AGEV instability, an analysis of the system phase portrait reveals that excessive tire slip angles can lead to

vehicle instability. Therefore, to ensure AGEV stability and maintain it within a certain range, it is necessary to impose constraints on the tire slip angles:

$$\begin{cases} \alpha_{f\tau,\min} \leq \alpha_{f\tau} \leq \alpha_{f\tau,\max} \\ \alpha_{r\tau,\min} \leq \alpha_{r\tau} \leq \alpha_{r\tau,\max} \end{cases} \quad (26)$$

Subsequently, by solving the optimization problem, the initial control input u_0 for ADRC is obtained. It is determined by solving the optimization problem based on the established model. However, during the model formulation, many nonlinear terms are linearized to simplify the problem and enhance computational speed. Next, we proceed to design ADRC to estimate and compensate for these disturbances.

Choosing Y , φ , and ω_r as state variables and applying coordinate transformation, the AGEV path tracking model (20) can be expressed as the following equation:

$$\begin{cases} \dot{Y} = \mu_x \sin \varphi + v_y \cos \varphi \\ \dot{\varphi} = \omega_r \\ \dot{\omega}_r = f(\varphi, \omega_r) + \gamma(t) + \frac{\bar{N}_{C_f l_f}}{I_z} \delta_f \\ f(\varphi, \omega_r) = \frac{\bar{N}_{C_f l_f}}{I_z} \left(-\beta - \frac{\omega_r l_f}{\mu}\right) - \frac{\bar{N}_{C_f l_f} N_{C_r}}{I_z} \left(\frac{\omega_r l_r}{\mu} - \beta\right) \end{cases} \quad (27)$$

where $\gamma(t)$ represents the disturbance term. It encompasses both external disturbances (such as air resistance disturbance, longitudinal velocity change disturbance, and road friction coefficient disturbance) and internal disturbances (such as parameter perturbation disturbance, signal delay disturbance, and system linearization disturbance) of the system.

Lateral position and yaw angle, controlled by manipulating the front wheel steering angle, constitute an underactuated system. To further enhance control effectiveness and utilize the ADRC controller effectively, we appropriately reduced the dimensionality of the system. Construct a function that satisfies the condition where the lateral error y_e converges to 0 as the vehicle's yaw angle φ approaches the desired yaw angle φ_{desire} . This way, we have reduced the original problem's dimensionality and transformed it into a vehicle yaw angle control problem. Here is the modified version of the first term in Equation (20):

$$\dot{Y} = \mu_x \sin \varphi + v_y \cos \varphi = \sqrt{\mu_x^2 + v_y^2} \sin(\varphi + \beta) \quad (28)$$

Note that vehicle state, such as the side-slip angle of center can, be estimated using an online estimation method and observer [25–27]. When the AGEV is traveling at high speeds, the center of the side-slip angle can have a significant impact on the AGEV's stability. If the side-slip angle is not compensated for the actual trajectory of the AGEV during, its travel can exhibit steady-state errors in comparison to the reference path.

$$\theta = \Delta\eta_0 \tanh(\Delta\eta_1 * y_e) + \varphi_e + \beta \quad (29)$$

where:

$$\begin{cases} 0 < \Delta\eta_0 < \pi \\ 0 < \Delta\eta_1 < \pi \\ \lim_{\theta \rightarrow 0} (\Delta\eta_0 \tanh(\Delta\eta_1 * y_e)) = 0 \\ \lim_{\theta \rightarrow 0} (\varphi_e + \beta) = 0 \end{cases}$$

Choose a Lyapunov function:

$$V = \frac{y_e^2}{2} \quad (30)$$

Differentiate V :

$$\dot{V} = y_e \dot{y}_e = y_e \sqrt{\mu_x^2 + v_y^2} \sin(\theta - \Delta\eta_0 \tanh(\Delta\eta_1 * y_e)) \quad (31)$$

When θ approaches 0, the equation can be written in the following form:

$$\lim_{\theta \rightarrow 0} \dot{V} = y_e \sqrt{\mu^2 + v^2} \sin(-\Delta\eta_0 \tanh(\Delta\eta_1 * y_e)) \quad (32)$$

Using deduction, we can obtain:

$$\begin{cases} -\Delta\eta_0 < -\Delta\eta_0 \tanh(\Delta\eta_1 y_e) < 0 \\ \sin(-\Delta\eta_0 \tanh(\Delta\eta_1 * y_e)) > 0 \end{cases} \quad (33)$$

where:

$$\begin{cases} y_e > 0 \\ 0 < \Delta\eta_0 < \pi \end{cases}$$

Hence, by referring to Equations (31) and (32), we can deduce: $\dot{V} < 0$

When $y_e = 0$ and $0 < \Delta\eta_0 < \pi$, we can obtain $\dot{V} = 0$.

Finally, we can arrive at:

$$\begin{cases} \dot{V} \leq 0 \\ \lim_{\theta \rightarrow 0} y_e = 0 \end{cases} \quad (34)$$

Next, according to Equation (35), we can derive $\varphi_e + \beta \rightarrow 0$. Since the bounded hyperbolic tangent function \tanh is employed here, $\Delta\eta_0$ can be utilized to restrict the maximum yaw angle during vehicle travel.

Finally, by setting $\theta = 0$, we can obtain the desired yaw angle:

$$\varphi_{desire} = -\Delta\eta_0 \tanh(\Delta\eta_1 y_e) - \beta + \varphi_{ref} \quad (35)$$

Assume that:

$$\varphi = z_{k1}, \dot{\varphi} = z_{k2} \quad (36)$$

The system which is equivalent to (20) is as follows:

$$\begin{cases} \dot{z}_{k1} = z_{k2} \\ \dot{z}_{k2} = f(z_{k1}, z_{k2}) + bu \\ y = z_{k1} \end{cases} \quad (37)$$

Using this approach, the underactuated problem in the lateral path tracking control of AGEV can be addressed by controlling the yaw angle φ to track the desired yaw angle φ_{desire} , calculated using y_e and φ_e .

In the context of ADRC, the ESO is introduced to handle disturbances. It is capable of estimating all system internal and external disturbances beyond just the state variables. Construct the extended state variable:

$$z_{k3} = f(z_{k1}, z_{k2}) \quad (38)$$

Through this approach, Equation (45) can be re-written in a form that includes the extended state variable.

$$\begin{cases} \dot{z}_{k1} = z_{k2} \\ \dot{z}_{k2} = z_{k3} + bu \\ \dot{z}_{k3} = \Delta\tilde{\zeta}_{dis}(t) \\ y = z_{k1} \end{cases} \quad (39)$$

$\Delta\tilde{\zeta}_{dis}(t)$ is bounded in reality.

Taking the sampling time as T_s and using the forward Euler method, we transform Equation (39) into its discrete form.

$$\begin{cases} z_{d,k1}(k+1) = z_{d,k1}(k) + T_s z_{d,k2}(k) \\ z_{d,k2}(k+1) = z_{d,k2}(k) + T_s(z_{d,k2}(k) + bu(k)) \\ z_{d,k3}(k+1) = z_{d,k3}(k) + T_s \Delta \bar{\xi}_{dis}(k) \\ y(k+1) = z_{d,k1}(k+1) \end{cases} \quad (40)$$

Based on Equation (40), we design the TD module.

$$\begin{cases} p_{T1}(k+1) = p_{T1}(k) + T_s p_{T2}(k) \\ p_{T2}(k+1) = p_{T2}(k) + T_s \bar{Q}(k) \\ \bar{Q}(k+1) = -\chi(\chi(p_{T1}(k) - p_{T0}(k)) + 2p_{T2}(k)) \end{cases} \quad (41)$$

Subsequently, we design the ESO to estimate the internal and external disturbances in the system.

$$\begin{cases} e = z_{e,k1} - y \\ \dot{z}_{e,k1} = z_{e,k2} - \lambda_e e \\ \dot{z}_{e,k2} = z_{e,k3} - \beta_e fal_{eso}(e, \zeta_{eso,1}, \kappa_{eso}) \\ \dot{z}_{e,k3} = -\gamma_e fal_{eso}(e, \zeta_{eso,2}, \kappa_{eso}) \end{cases} \quad (42)$$

where:

$$fal_{eso}(e, \zeta_{eso,i}, \kappa_{eso}) = \begin{cases} \frac{e}{\kappa_{eso}^{1-\zeta_{eso,i}}}, |e| \leq \kappa_{eso} \\ |e| \operatorname{sgn}(e), |e| > \kappa_{eso} \end{cases}$$

Transform Equation (42) into its discrete form:

$$\begin{cases} e(k+1) = z_{e,k1}(k) - y(k+1) \\ z_{e,k1}(k+1) = z_{e,k1}(k) + T_s(z_{e,k2}(k) - \lambda_e e(k+1)) \\ z_{e,k2}(k+1) = z_{e,k2}(k) + T_s(z_{e,k3}(k) - \beta_e fal_{eso}(e(k+1), \zeta_{eso,1}, \kappa_{eso}) + \tilde{b}u(k)) \\ z_{e,k3}(k+1) = z_{e,k3}(k) + T_s(-\gamma_e fal_{eso}(e(k+1), \zeta_{eso,2}, \kappa_{eso})) \end{cases} \quad (43)$$

where $\lambda_e, \beta_e, \gamma_e$ are the ESO gains. Next, we analyze the stability of the ESO.

We rewrite Equation (42) in matrix form:

$$\dot{\bar{Z}}_e = -\bar{A}_e(e)\bar{Z}_e \quad (44)$$

where:

$$\bar{Z}_e = \begin{bmatrix} z_{e,k1} \\ z_{e,k2} \\ z_{e,k3} \end{bmatrix}, \bar{A}_e = \begin{bmatrix} \lambda_e & -1 & 0 \\ \beta_e \omega_1 & 0 & -1 \\ \gamma_e \omega_2 & 0 & 0 \end{bmatrix}, \omega_i = \frac{fal_{eso}(e, \zeta_{eso,p}, \kappa_{eso})}{e}, p = 1, 2$$

Because $0 < \zeta_{eso,p} < 1, p = 1, 2, \omega_1, \omega_2$ is bounded.

For the aforementioned system, if there exists a matrix \bar{M}_e in the following form and the main diagonal elements of the matrix \bar{M}_e are positive such that the matrix $\bar{N}_{eso} = \bar{M}_{eso}\bar{A}_e(e)$ is positive definite symmetric, then the solution of the above system is Lyapunov stable.

$$\bar{N}_{eso} = \bar{M}_{eso}\bar{A}_e(e) = \begin{bmatrix} n_{eso,11} & -m_{eso,11} & -m_{eso,12} \\ n_{eso,21} & m_{eso,12} & -m_{eso,22} \\ n_{eso,31} & m_{eso,13} & m_{eso,23} \end{bmatrix} \quad (45)$$

To prove that the matrix \bar{N}_e is positive definite and symmetric, it is sufficient to ensure that its symmetric elements are equal and that all three leading principal minors have determinants greater than zero. We can transform this into the following equivalent conditions:

$$\left\{ \begin{array}{l} m_{eso,13} = -m_{eso,22} \\ n_{eso,31} = -m_{eso,12} \\ n_{eso,21} = -m_{eso,11} \\ n_{eso,11} > 0 \\ \left| \begin{array}{cc} n_{eso,11} & -m_{eso,11} \\ n_{eso,21} & m_{eso,12} \end{array} \right| > 0 \\ \left| \begin{array}{ccc} n_{eso,11} & -m_{eso,11} & -m_{eso,12} \\ n_{eso,21} & m_{eso,12} & -m_{eso,22} \\ n_{eso,31} & m_{eso,13} & m_{eso,23} \end{array} \right| > 0 \end{array} \right. \quad (46)$$

Let $m_{eso,11} = 1, m_{eso,22} = \lim \varepsilon_e \rightarrow 0$; we can obtain:

$$m_{eso,23} = \frac{1 + \varepsilon_e \bar{\lambda}_e^2 + \varepsilon_e \bar{\beta}_e \bar{\lambda}_e - \varepsilon_e \bar{\gamma}_e \bar{\lambda}_e}{(\bar{\lambda}_e \bar{\beta}_e - \bar{\gamma}_e) \bar{\lambda}_e} \quad (47)$$

Due to this, $\lim \varepsilon_e \rightarrow 0$, and we can obtain:

$$n_{eso,11} = \bar{\lambda}_e + \frac{\bar{\beta}_e^2 \bar{\lambda}_e}{(\bar{\lambda}_e \bar{\beta}_e - \bar{\gamma}_e)} \quad (48)$$

As long as it is ensured, we can obtain:

$$\left| \begin{array}{cc} n_{eso,11} & -m_{eso,11} \\ n_{eso,21} & m_{eso,12} \end{array} \right| = n_{eso,11} m_{eso,12} - 1 \quad (49)$$

$$\left| \begin{array}{ccc} n_{eso,11} & -m_{eso,11} & -m_{eso,12} \\ n_{eso,21} & m_{eso,12} & -m_{eso,22} \\ n_{eso,31} & m_{eso,13} & m_{eso,23} \end{array} \right| \quad (50)$$

$$= n_{eso,11} (m_{eso,12} m_{eso,23} - m_{eso,22}^2) - 2m_{eso,11} m_{eso,12} m_{eso,22} - m_{eso,11}^2 m_{eso,23} - m_{eso,12}^3$$

After rearranging, we obtain:

$$\frac{\bar{\gamma}_e}{(\bar{\lambda}_e \bar{\beta}_e - \bar{\beta}_e)^2 \bar{\lambda}_e} > 0 \quad (51)$$

In conclusion, a matrix satisfying the aforementioned conditions can be found, and the solution of the above system is Lyapunov stable. The three state variables of the extended state observer can track the system's state variables.

For the NLFSE part, to improve control effectiveness, we substitute the previously designed MPC.

We obtain the final output of the controller:

$$u = \frac{\Delta \delta_{p,f} - z_{e,k3}}{\tilde{b}} \quad (52)$$

4. Simulation and Results

This section simulates and verifies the feasibility of the proposed active disturbance rejection controller (ADRC) for the trajectory-following of AGEV. The simulation framework is constructed using MATLAB/Simulink, and high-precision vehicle dynamics models are provided by Carsim[®] software. The key parameters of the vehicle are listed in Table 1. The simulation scenarios include double lane change (DLC) and serpentine science with a forward speed of 54 km/h. For comparison, the performance of the proposed controller is

compared with that of the linear quadratic regulator controller (LQR) and model predictive controller (MPC).

Table 1. The key parameters of the vehicle.

Parameter	Scale	Unit
m	1270	kg
I_z	1536.7	kg*m ²
N_{cf}	[87,445, 108,533]	N/rad
N_{cr}	[68,446, 89,664]	N/rad
l_f	1.015	m
l_r	1.895	m
l_z	0.54	m
r	0.325	m

4.1. Double Lane Change Science

The simulation results of the double lane change are presented in Figures 2–7. Figures 2 and 3 depict the global trajectory and lateral error during the DLC tracking process, respectively. Tracking error is one of the most crucial performance metrics in AGEV path-tracking control. From Figure 2, it can be inferred that the tracking performance of the ADRC-MPC controller is significantly superior to that of the MPC and LQR. The maximum error of the MPC and LQR controllers exceeds 0.05 (m), whereas the ADRC-MPC’s error is only 0.04 (m). Furthermore, there is a noticeable reduction in the magnitude of lateral error fluctuations. It can be observed that under the same controller parameters, the tracking control results based on ADRC-MPC exhibit lower overshoot peaks. These findings indicate that ADRC-MPC outperforms MPC and LQR in terms of tracking performance on DLC roads.

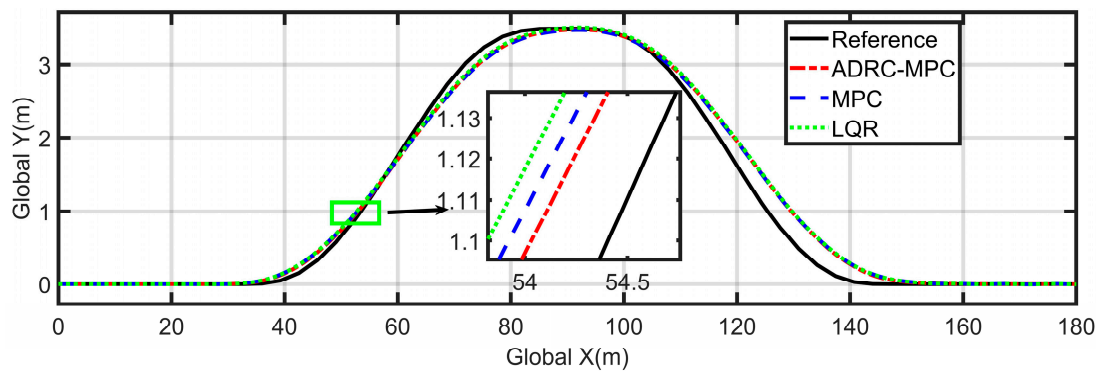


Figure 2. Global trajectories of three controllers under the DLC scene.

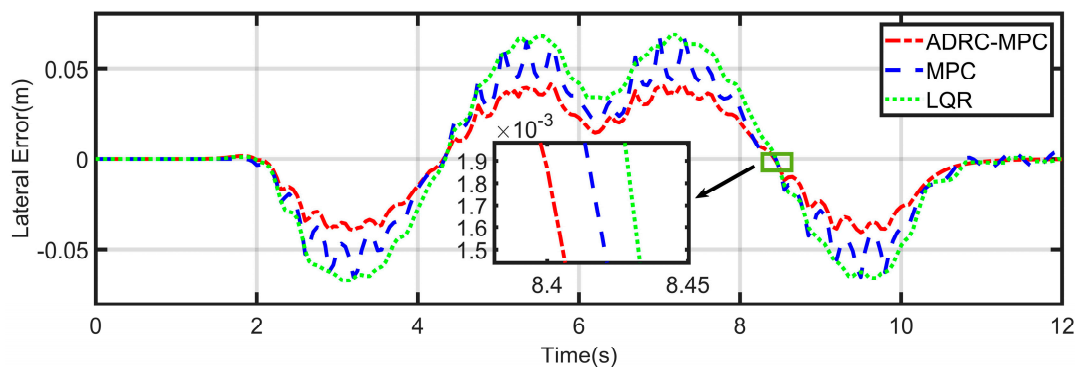


Figure 3. Lateral errors of three controllers under the DLC scene.

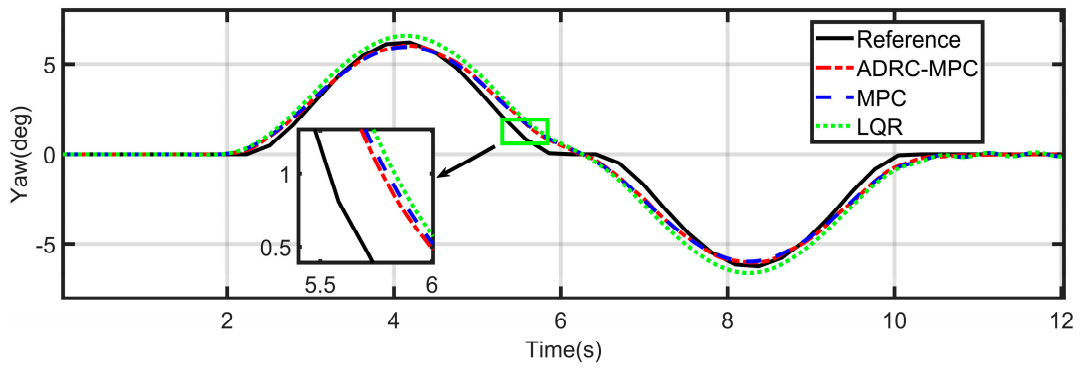


Figure 4. Yaw of three controllers under the DLC scene.

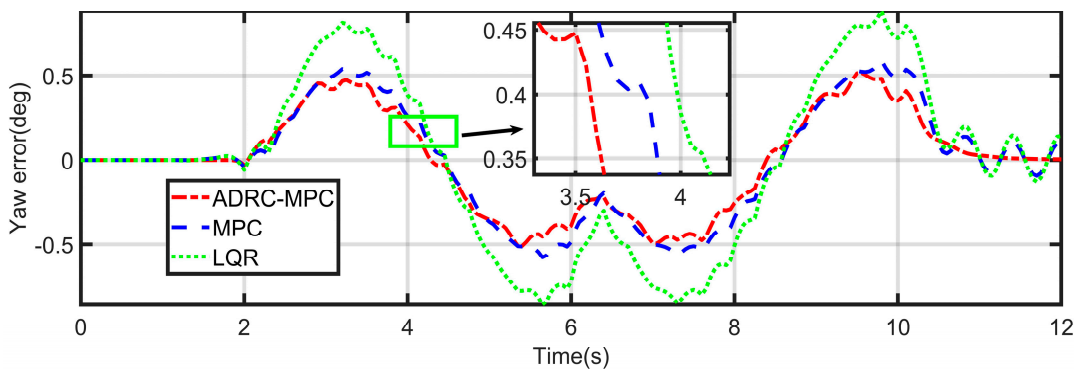


Figure 5. Yaw errors of three controllers under the DLC scene.

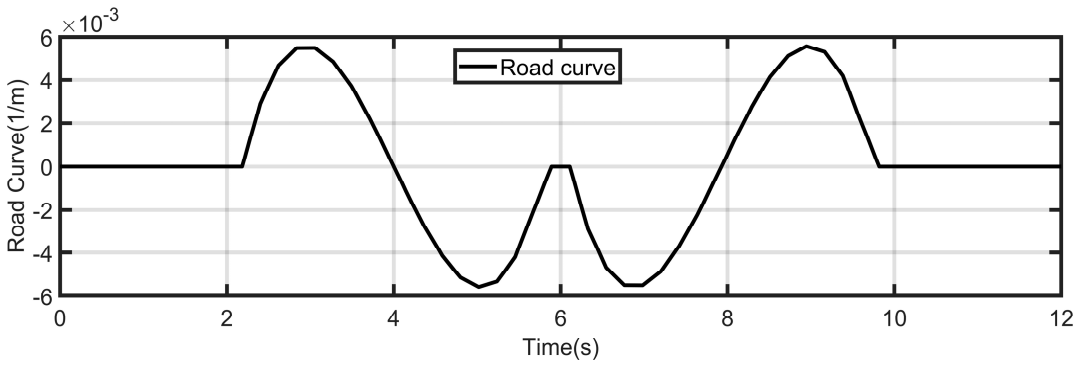


Figure 6. The curvature of the road under the DLC scene.

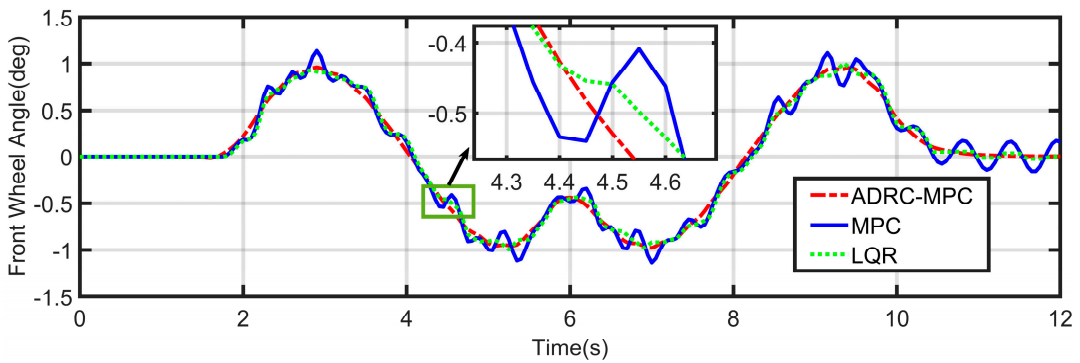


Figure 7. Front wheel angles of three controllers under the DLC scene.

Figure 4 illustrates that the three controllers can track the desired yaw angle. By zooming in locally, we can observe that ADRC-MPC’s tracking performance is superior to that of MPC and LQR.

The steering wheel angle affects the vehicle’s motion characteristics during its movement. The simulation results of this comparison are illustrated in Figure 8. It is evident that ADRC-MPC, MPC, and LQR exhibit similar longitudinal positions at the beginning of steering, but ADRC-MPC achieves a more stable output with a consistent steering wheel angle. The reduction in tracking errors and the improvement in output stability are both attributed to the effectiveness of ADRC. From this, it is evident that ADRC possesses excellent disturbance rejection capabilities, whether it pertains to disturbances originating from within the control system or from external sources. ADRC-MPC can significantly enhance the path-tracking performance of AGEV and the disturbance rejection capability of the control system.

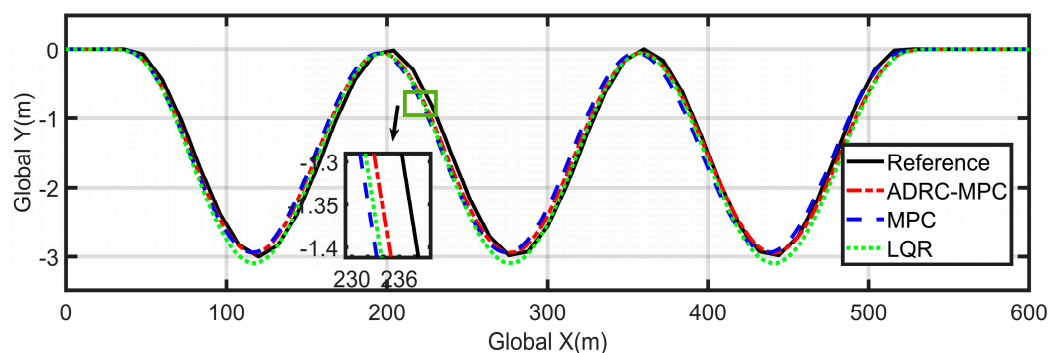


Figure 8. Global trajectories of three controllers under the serpentine scene.

4.2. Serpentine Scene

The simulation results of the serpentine lane are presented in Figures 8–13, including global trajectories, lateral errors, yaw, yaw errors, and road curvature. Figure 8 shows the global trajectories obtained from three controllers during serpentine tracking. All the controllers exhibited satisfactory performance. From Figure 9, it is evident that ADRC-MPC has reduced lateral error by half compared to MPC and LQR. The maximum lateral errors of MPC and LQR are approximately 0.05 (m) and the maximum lateral error of ADRC-MPC is approximately 0.025 (m). Moreover, ADRC-MPC stabilizes without generating minor oscillations in the end. It is worth noting that, compared to MPC and LQR, ADRC-MPC achieved a smaller maximum lateral error, indicating its superior tracking performance. The final fluctuations in the tracking performances of MPC and LQR can be attributed to disturbances arising from modeling inaccuracies and the short prediction horizon. However, ADRC-MPC achieves excellent control performance under the same model and prediction horizon, which better highlights the superior performance of the proposed controller.

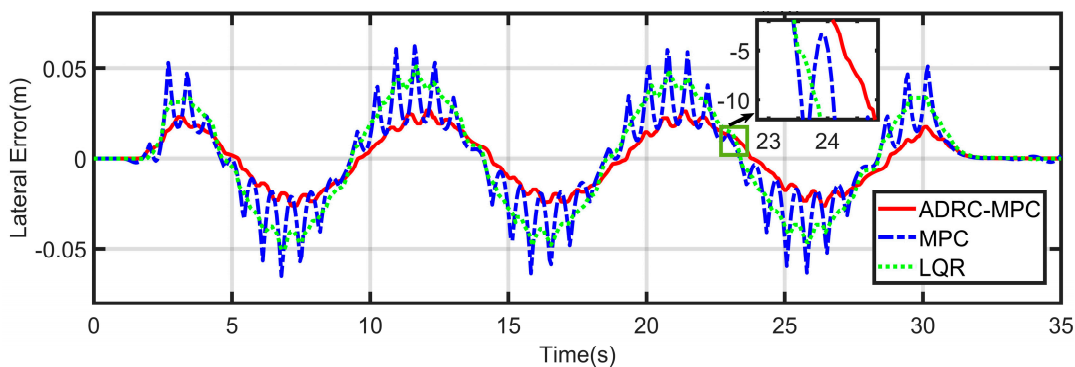


Figure 9. Lateral errors of three controllers under the serpentine scene.

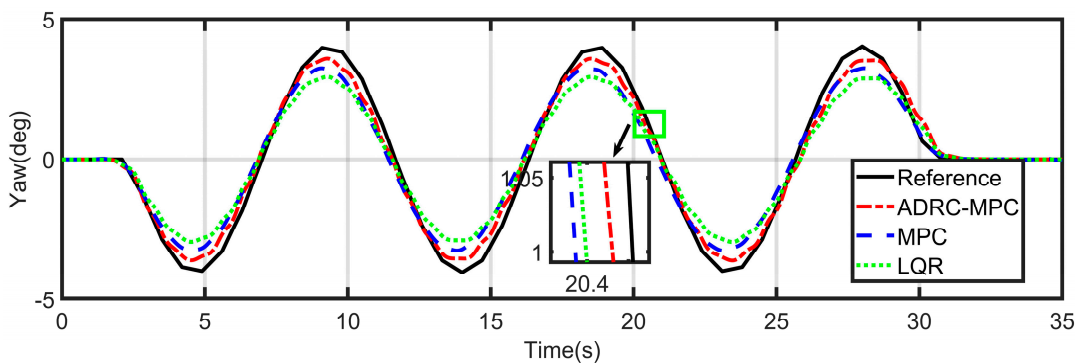


Figure 10. Yaw of three controllers under the serpentine scene.

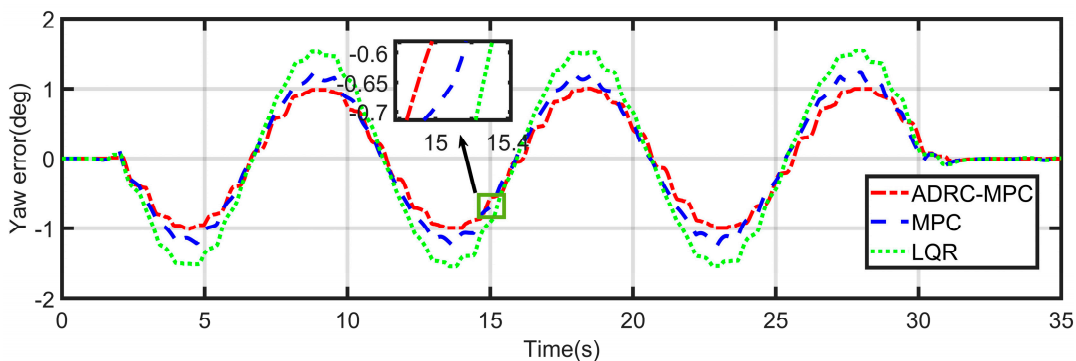


Figure 11. Yaw errors of three controllers under the serpentine scene.

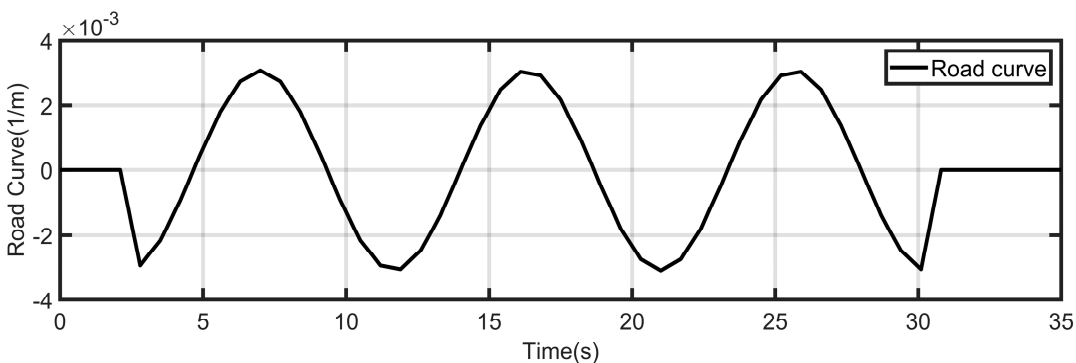


Figure 12. Curvature of the road under the serpentine scene.

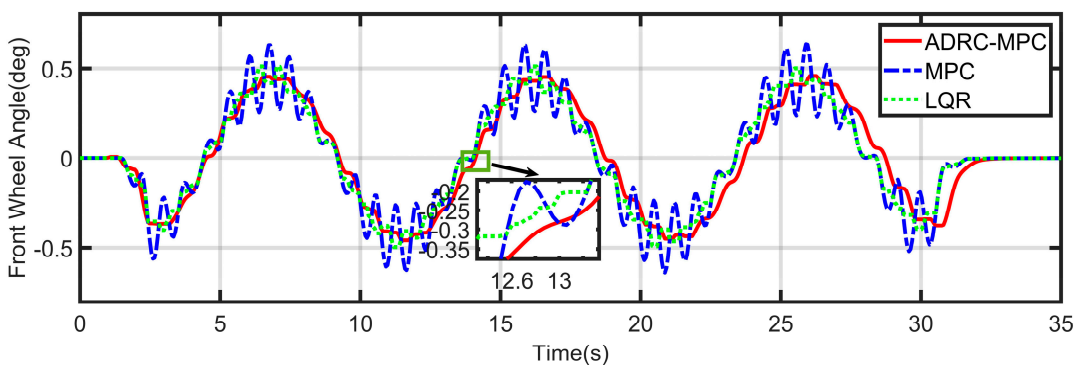


Figure 13. Front wheel angles of three controllers under serpentine scene.

Figure 10 illustrates that the three controllers can effectively track the desired yaw angle. Furthermore, by zooming in locally, we can observe that ADRC-MPC’s tracking performance is notably superior to that of MPC and LQR.

The road curve and longitudinal velocity of the serpentine scene are illustrated in Figures 12 and 14, respectively. Figure 13 indicates the front wheel angle of the three controllers. From Figure 13, it is evident that the control signal output of ADRC-MPC is significantly superior to that of MPC and LQR. This is because excessively small front wheel angles can result in sluggish system response, while excessively large front wheel angles can lead to significant overshooting. ADRC-MPC can compensate for control signal disturbances caused by system model. Hence, it can be demonstrated that the ADRC-MPC controller exhibits outstanding trajectory tracking capability and excellent disturbance-rejection ability.

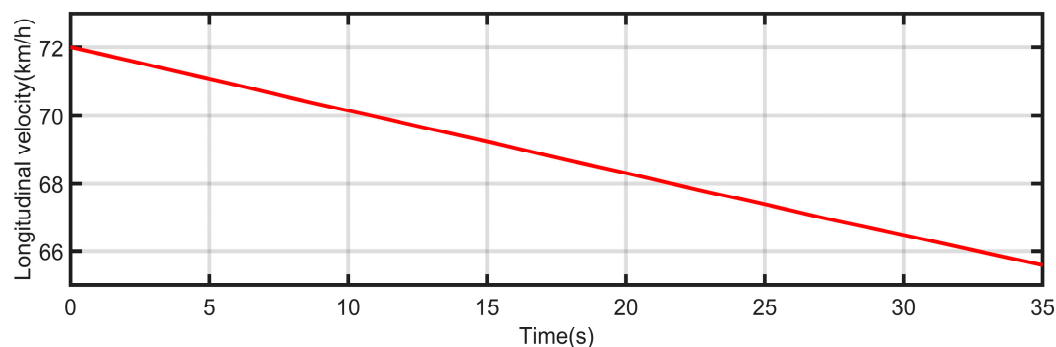


Figure 14. Longitudinal velocity of the serpentine scene.

5. Conclusions

To enhance the trajectory-following performance of the autonomous ground electric vehicles equipped with an active front steering system, the novel active disturbance rejection controller is designed to face the challenges of system uncertainties, system nonlinearities, and external disturbance. The vehicle dynamics trajectory-following model and its state space representation system are established, and the control-oriented vehicle-trajectory-following augmented system is also developed. The resulting active disturbance rejection controller of the vehicle trajectory-following system is finally designed with the Lyapunov stability theory. Simulations with different maneuvers are implemented to evaluate the designed controller in the Matlab/Simulink–CarSim[®] platform. Simulation results show that lateral errors and yaw errors managed by ADRC are much smaller than those of MPC and LQR. Additionally, ADRC exhibits the lowest fluctuations and overshoot peaks on tracking performance compared to MPC and LQR under double lane change and serpentine scenes. Simulation results indicate the effectiveness of the proposed controller. Although the difference between the simulation and the real physical system of actual vehicle is inevitable, the simulation results have a certain guidance for real trajectory-following system engineering design of AGEV. In the future, we will further research other advanced nonlinear and adaptive control techniques for trajectory following control of autonomous ground electric vehicles. In particular, we will perform vehicle hardware-in-the-loop tests and real vehicle road experiments to verify these control strategies.

Author Contributions: Conceptualization, X.J., H.L., Z.H., Z.L., Z.W. and N.V.O.I.; supervision, X.J. and Z.H.; conception and design, X.J., H.L. and Z.H.; collection and assembly of data, X.J., H.L., Z.L., Z.W. and N.V.O.I.; manuscript writing, X.J., H.L., Z.H., Z.L., Z.W. and N.V.O.I.; funding, X.J. All authors have read and agreed to the published version of the manuscript.

Funding: Shandong Innovation Competition Action Program under Grant 2022GDZB-TD01 and Foundation for State Key Laboratory of Automotive Simulation and Control under Grant 20181112.

Institutional Review Board Statement: Not applicable.

Informed Consent Statement: Not applicable.

Data Availability Statement: Not applicable.

Conflicts of Interest: The authors declare no conflict of interest.

Appendix A

Table A1. The essential parameters and symbols in the paper.

Parameter	Name	Parameter	Name
m_{AGEV}	vehicle mass	μ_x	longitudinal velocity
v_y	lateral velocity	φ	yaw angle
F_{f-y}	front axle lateral force	δ_f	front wheel steering angle
F_{f-x}	front axle longitudinal force	F_{r-x}	rear axle longitudinal force
y	longitudinal position	F_{r-y}	rear axle lateral force
I_z	moment of inertia	l_f	front wheelbase
l_r	rear wheelbase	v	vehicle speed
β	side-slip angle	F_y	lateral force
M_z	yaw torque	a_y	lateral acceleration
w_r	angular velocity	$\alpha_{f\tau}$	front wheel slip angle
$\alpha_{r\tau}$	rear wheel slip angle	\bar{N}_{C-f}	front wheel slip stiffness
\bar{N}_{C-r}	rear wheel slip stiffness	τ	model state error
y_e	lateral error	φ_e	yaw angle error
s	desire trajectory	$s_{TD,i}$	tracking signal of tracking differentiator
h	sampling time	τ	actual error
$z_{E,ki}$	state estimate of extended state observer	α_i	gain of the extended state observer
b	control gain coefficient	T_s	sampling time
x_k	state variables	$\tilde{x}_{p,k+i}$	predicted state variables
$u_{p,k+i}$	predicted control input	$\Delta\delta_{p,f}^{\max}$	maximum steering angle
$\Delta\delta_{p,f}^{\min}$	minimum steering angle	$\alpha_{i\tau,\max}$	maximum tire slip angle
$\alpha_{i\tau,\min}$	minimum tire slip angle	$\Delta\eta_i$	design parameters
θ	constructor	φ_{ref}	desired yaw angle
φ_{desire}	target yaw angle	z_{ki}	controlled state variables
$\Delta\zeta_{dis}$	estimated disturbance	$z_{d,ki}$	discrete controlled state variables
p_T	tracking signal of tracking differentiator	p_{T0}	set value of yaw angle
$\lambda_e, \beta_e, \gamma_e$	observer gains	$\kappa_{eso}, \zeta_{eso,i}$	controller parameters

References

- Deng, H.; Zhao, Y.; Nguyen, A.T.; Huang, C. Fault-tolerant predictive control with deep-reinforcement-learning-based torque distribution for four in-wheel motor drive. *IEEE/ASME Trans. Mechatron.* **2023**, *28*, 668–680. [CrossRef]
- Yassine, A.; Hossain, M.S.; Muhammad, G.; Guizani, M. Double auction mechanisms for dynamic autonomous electric vehicles energy trading. *IEEE Trans. Veh. Technol.* **2019**, *68*, 7466–7476. [CrossRef]
- Jin, X.; Wang, J.; He, X.; Yan, Z.; Xu, L.; Wei, C.; Yin, G. Improving vibration performance of electric vehicles based on in-wheel motor-active suspension system via robust finite frequency control. *IEEE Trans. Intell. Transp. Syst.* **2023**, *24*, 1631–1643. [CrossRef]
- Jin, X.; Wang, J.; Yan, Z.; Xu, L.; Yin, G.; Chen, N. Robust vibration control for active suspension system of in-wheel-motor-driven electric vehicle via μ -synthesis methodology. *ASME Trans. J. Dyn. Syst. Meas. Control.* **2022**, *144*, 051007. [CrossRef]
- Barari, A.; Saraygord Afshari, S.; Liang, X. Coordinated control for path-following of an autonomous four in-wheel motor drive electric vehicle. *Proc. Inst. Mech. Eng. C J. Mech. Eng.* **2022**, *236*, 6335–6346. [CrossRef] [PubMed]
- Gözü, M.; Ozkan, B.; Emirler, M.T. Disturbance observer based active independent front steering control for improving vehicle yaw stability and tire utilization. *Int. J. Autom. Technol.* **2022**, *23*, 841–854. [CrossRef]
- Mousavinejad, E.; Han, Q.; Yang, F.; Zhu, Y.; Vlacic, L. Integrated control of ground vehicles dynamics via advanced terminal sliding mode control. *Veh. Syst. Dyn.* **2017**, *55*, 268–294. [CrossRef]
- Ghazali, M. Path-following and tire loss investigation of a front in-wheel-drive electric vehicle with off-centre CG. *Mech. Mach. Theory.* **2023**, *189*, 105422. [CrossRef]
- Wang, G.; Liu, Y.; Li, S.; Tian, Y.; Zhang, N.; Cui, G. New integrated vehicle stability control of active front steering and electronic stability control considering tire force reserve capability. *IEEE Trans. Veh. Technol.* **2021**, *70*, 2181–2195. [CrossRef]
- Fnadi, M.; Plumet, F.; Benamar, F. Model predictive control based dynamic path tracking of a four-wheel steering mobile robot. In Proceedings of the IEEE/RSJ International Conference on Intelligent Robots and Systems (IROS), Macau, China, 4–8 November 2019; pp. 4518–4523.
- Fnadi, M.; Du, W.; Plumet, F.; Benamar, F. Constrained Model Predictive Control for dynamic path tracking of a bi-steerable rover on slippery grounds. *Control Eng. Pract.* **2021**, *107*, 104693. [CrossRef]
- Lee, M.Y.; Chen, B.S. Robust H-infinity network observer-based attack-tolerant path tracking control of autonomous ground vehicle. *IEEE Access.* **2022**, *10*, 58332–58353. [CrossRef]

13. Ahmed, M.; El-Gindy, M.; Lang, H. Path-following enhancement of an 8 × 8 combat vehicle using active rear axles steering strategies. *Proc. Inst. Mech. Eng. K J. Mul. Dyn.* **2021**, *235*, 539–552. [[CrossRef](#)]
14. Nguyen, A.T.; Sentouh, C.; Zhang, H.; Popieul, J.C. Fuzzy static output feedback control for path following of autonomous vehicles with transient performance improvements. *IEEE Trans. Intell. Transp. Syst.* **2019**, *21*, 3069–3079. [[CrossRef](#)]
15. Oh, K.; Seo, J. Development of a Sliding-Mode-Control-Based Path-Tracking Algorithm with Model-Free Adaptive Feedback Action for Autonomous Vehicles. *Sensors* **2022**, *23*, 405. [[CrossRef](#)] [[PubMed](#)]
16. Jin, X.; Wang, Q.; Yan, Z.; Yang, H. Nonlinear robust control of trajectory-following for autonomous ground electric vehicles with active front steering system. *AIMS Math.* **2023**, *8*, 11151–11179. [[CrossRef](#)]
17. Fnadi, M.; Alexandre dit Sandretto, J. Experimental validation of a guaranteed nonlinear model predictive control. *Algorithms* **2021**, *14*, 248. [[CrossRef](#)]
18. Han, J. From PID to active disturbance rejection control. *IEEE Trans. Ind. Electron.* **2009**, *56*, 900–906. [[CrossRef](#)]
19. Lu, W.; Li, Q.; Lu, K.; Lu, Y.; Guo, L.; Yan, W.; Xu, F. Load adaptive PMSM drive system based on an improved ADRC for manipulator joint. *IEEE Access* **2021**, *9*, 33369–33384. [[CrossRef](#)]
20. Lin, P.; Wu, Z.; Fei, Z.; Sun, X. A Generalized PID Interpretation for High-Order LADRC and Cascade LADRC for Servo Systems. *IEEE Trans. Ind. Electron.* **2021**, *69*, 5207–5214. [[CrossRef](#)]
21. Yuan, C.; Zhou, X.; Ma, Y. DC Bus Voltage Control of Wind Power Inverter Based on First-Order LADRC. *IEEE Access* **2021**, *10*, 3263–3274. [[CrossRef](#)]
22. Xia, Y.; Fu, M.; Li, C.; Pu, F.; Xu, Y. Active disturbance rejection control for active suspension system of tracked vehicles with gun. *IEEE Trans. Ind. Electron.* **2017**, *65*, 4051–4060. [[CrossRef](#)]
23. Li, Y.; Zhang, C.; Song, J.; Li, X.; Duan, B. An active disturbance rejection control strategy for a three-phase isolated matrix rectifier. *IEEE Trans. Transport. Electrification.* **2021**, *8*, 820–829. [[CrossRef](#)]
24. Xu, L.; Ma, J.; Guo, D.; Xie, A.; Song, D. Backstepping sliding-mode and cascade active disturbance rejection control for a quadrotor UAV. *IEEE/ASME Trans. Mechatron.* **2020**, *25*, 2743–2753. [[CrossRef](#)]
25. Jin, X.; Yang, J.; Xu, L.; Wei, C.; Wang, Z.; Yin, G. Combined Estimation of Vehicle Dynamic State and Inertial Parameter for Electric Vehicles Based on Dual Central Difference Kalman Filter Method. *Chin. J. Mech. Eng.* **2023**, *36*, 1–16. [[CrossRef](#)]
26. Baffet, G.; Charara, A.; Lechner, D.; Thomas, D. Experimental evaluation of observers for tire–road forces, sideslip angle and wheel cornering stiffness. *Veh. Syst. Dyn.* **2008**, *46*, 501–520. [[CrossRef](#)]
27. Fnadi, M.; Plumet, F.; Benamar, F. Nonlinear tire cornering stiffness observer for a double steering off-road mobile robot. In Proceedings of the International Conference on Robotics and Automation (ICRA), Montreal, QC, Canada, 20–24 May 2019; pp. 7529–7534.

Disclaimer/Publisher’s Note: The statements, opinions and data contained in all publications are solely those of the individual author(s) and contributor(s) and not of MDPI and/or the editor(s). MDPI and/or the editor(s) disclaim responsibility for any injury to people or property resulting from any ideas, methods, instructions or products referred to in the content.